1-1-2018

Characterization and electrochemical performance of Manganese oxide with carbon nano tubes as negative electrode for lithium batteries

Atef Y. Shenouda
Central Metallurgical Research and Development Institute, ayshenouga@yahoo.com

Haipeng Guo
University of Wollongong, hg476@uowmail.edu.au

Jiazhao Wang
University of Wollongong, jiazhao@uow.edu.au

Characterization and electrochemical performance of Manganese oxide with carbon nano tubes as negative electrode for lithium batteries

Characterization and electrochemical performance of Manganese oxide with carbon nano tubes as negative electrode for lithium batteries

Characterization and electrochemical performance of Manganese oxide with carbon nano tubes as negative electrode for lithium batteries

Atef YShenouda[1], Haipeng Guo[2] and Jiazhao Wang[2]

[1]Central Metallurgical Research and Development Institute (CMRDI), Tebbin, P.O. Box 87 Helwan, Egypt.

[2] Institute for Superconducting and Electronic Materials (ISEM), Innovation Campus, University of Wollongong, NSW, Australia.

E-mail: ayshenouda@gmail.com

Abstract. Different ratios of Mn_3O_4/CNT (carbon nano tubes) samples were prepared by ultrasonic and hydrothermal reactions. The added ratios of CNT: Mn wt./wt. were 0, 5, 15, 25, 35 and 50%. The phases of the samples were identified by X-ray diffraction (XRD). The particle morphology was studied with a field emission scanning electron microscope (FESEM). The lowest charge transfer resistance, R_{ct} was 19.18 Ω with cell of Mn_3O_4/35% CNT. For Li/ Mn_3O_4- 35% CNT cell, the specific discharge capacity was about **688** $mAhg^{-1}$ after **100** cycles, which was the highest value among the other cells at discharge current density $0.02Acm^{-2}$.

Keywords: Lithium battery anode, Mn_3O_4/CNT.

1. Introduction

Small and Portable electronic devices such as laptops, mobile telephones, camcorders, etc. use Lithium-ion battery (LIB). They are considered the essential electric power component for these devices due to their excellent properties like long durability, high energy density, easily handling and safe for the environment. A variety of metals and metal oxides are intensively studied in order to obtain high-capacity anode materials for LIBs [1–4].

The synthesis of Mn_3O_4 with CNT was reported in some researches [5–16]. Manganese oxide with multi-wall carbon nanotubes (MWCNTs) was prepared by hydrothermal method using CH_3COONa. Mn3O4 nano-crystals were introduced inside MWCNTs [6]. The nanocomposite performed good cycling stability and rate capability. The initial reversible capacity was 1380 mAh g−1 at a current density of 100 mAg^{-1}. The reversible cycle discharge capacity was 592 $mAhg^{-1}$ after 50 cycles. The good performance of Mn_3O_4/MWCNTs was discussed.

It was reported that Mn_3O_4nano-particles anchored on continuous super-aligned carbon nanotube (SACNT) films were obtained by decomposition of $Mn(NO_3)_2$[9]. The electrochemical performance of the Mn_3O_4/SACNT composite electrode is greatly affected by the grain size of Mn_3O_4. For smaller particle size, the electrode displayed smaller voltage hysteresis and much improved reversibility and rate capability. Mn_3O_4 with particle size of less than 10 nm inside the Mn_3O_4/SACNT electrodes showed a capacity of 342 mAh g^{-1} at 10 C. This composite material has more advantages than the commercial graphite anode and promising in practical applications.

Mn_3O_4 / CNT was synthesized by a simple hydrothermal method [10]. MnO / CNT was obtained by heating Mn_3O_4/CNTs at 500°C for 3 h in flowing Ar/H_2. After 30 cycles, the discharge capacity of Mn3O4 electrode is only 280 $mAhg^{-1}$, whereas that of Mn_3O_4/CNTs electrode can still remain with 548 mAh g-1 at current density 100 mAh g^{-1}. While MnO / CNT cell has 600 vs. 200 mAh g^{-1} for MnO. The manganese oxide/CNTs composites has stable cyclability, good rate performance and promising anode materials.

Carbon nanofiber/Mn3O4 (CNF/Mn_3O_4) coaxial nano-fibers with a three-dimensional (3D) structure were prepared for lithium ion batteries by electrophoretic deposition on an electrospun CNF cathode followed by heat treatment in air [11]. The CNF/Mn_3O_4 coaxial nanocables showed a high reversible capacity of 760 mAh g^{-1} at 100 mA g^{-1} even after 50 charge discharge cycles without capacity fading.

A facile and green chemistry route was developed to prepare a Mn_3O_4 nanoparticles (NPs)/ exfoliated graphite (EG) composite by artfully tuning the traditional fabrication process of EG [12]. During this treatment, Mn_3O_4-NPs with high crystallinity and uniform dimension of 7 nm were found to be homogeneously and firmly anchored on the surface of EG. The composite as an anode material of Li-ion batteries exhibited suitable specific discharge capacity of 655 $mAhg^{-1}$ extending to more than 100 cycles.The aim of this work is to study the effect of different ratios of CNT on the performance of Mn – oxide in lithium cell as there is a need to study effect of the CNT ratios according to the reported literature.

2. Experimental

2.1. Materials preparation and characterization

Different ratios of carbon nano tubes (CNT), (99%, Ad-Nano Technologies Private Limited, India) 0, 5, 15, 25, 35 and 50% were added to stoichiometric amounts of $(CH_3CO_2)_2Mn.4H_2O$ (Aldrich, 99.5%) dissolved in distilled water to prepare the samples. The ratios of CNT were calculated as Mn: C. The suspended CNT of each mixture solution was stirred and heat-treated at 80°C for 2 hours. Furthermore, the mixture was exposed toultrasonic vibration for one hour. After that, the mixture was transferred to an autoclave vessel (250 cm^3) and heat-treated at 200°C for 24 hours.

The crystalline phases of the samples were identified by X-ray diffraction (XRD) using a step size of 0.02° and at a scanning rate of 0.16°/min on a Brucker axis D8 diffractometer with crystallographic data software Topas 2 using Cu Kα (λ = 1.54056 Å) radiation operating at accelerating voltage and applied current were 40 kV and 80 mA, respectively. The diffraction data was recorded for 2θ values between 10° and 80°. The particle morphology was studied with a field emission scanning electron microscope (FESEM QUANTAFEG 250). The magnetic properties of some of the samples powders were measured at room temperature using a vibrating sample magnetometer (VSM, 7410 Lakeshore, USA) in a maximum applied field of 20 kOe.

2.2. Electrochemical measurements

The homogeneous slurry used to form the electrodes was composed of 85 wt% active materials, 10 wt% acetylene black, and 5 wt% sodium carboxy methyl cellulose (SCMC) as binder dissolved in distilled water. It was then spread onto Cu foil substrates. The area of each coated electrode was 1 cm^2. The electrodes were dried in a vacuum oven at 110°C for 12 h. The electrodes were then pressed at a pressure of 2000 kg/cm2. The active material loading was about 5 mg for each individual electrode. CR2032 coin cells were then assembled in an argon filled glove box (Mbraun, Unilab, Germany), using lithium metal foil as the counter electrode. The electrolyte was 1M $LiPF_6$ in a mixture of ethylene carbonate (EC) and dimethyl carbonate (DMC) (1:1 by volume, provided by MERCK). The cells were galvanostatically charged and discharged over a voltage range of 0.0–3 V using a current of 0.02 A/ cm^2 for both processes. Cyclic voltammetry (CV) measurements were performed using a Multi-stat CHI660 Electrochemical Workstation at a 0.1 mVs^{-1} scanning rate, and

the potential windows were 0 and 3 V versus Li/Li+ electrode. The Galvanostatic charge-discharge measurements were performed on a Neware Battery Tester. The frequency range of the AC impedance measurement was 1MHz – 10 mHz and10 mV amplitude.

3. Results and Discussion

3.1 Structural Characterization

X-ray diffraction patterns of the manganese oxide and manganese oxide with CNT samples show suitable crystallinity as shown in Figure 1. Samples diffraction peaks exhibited good crystalline structures. Their structures were indexed to the tetragonal system with space group of I41/amd (JCPDS No. 24–0734). The peak at 2θ =26.4° can be achieved to (002) of the hexagonal carbon in CNT (JCPDS No. 26–1079). Mainly, there is no other phase that observed in the patterns. The main diffractions are (103), (211) and (224) for Mn3O4. The crystallite sizes of Mn_3O_4, Mn_3O_4 with 25% CNT and Mn3O4 with 35% CNT are 22.07, 13.58 and 11.03 nm, respectively at 2 θ =37° according to the Debye-Scherrer equation [2,3]:

$$L = 0.94 \lambda / w \cos \theta \quad (1)$$

where θ and w are the Bragg angle and the full width at half maximum peak, measured in radians, of each diffraction peak, respectively. Also, λ is the X-ray wavelength (1.54056Å), and L is the effective particle or grain size.

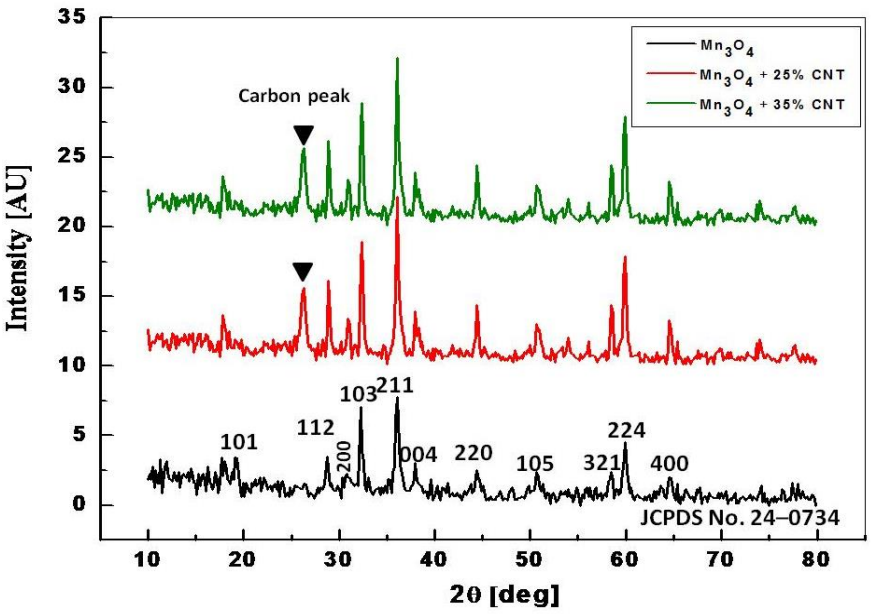

Figure 1. XRD of (a) Mn_3O_4, (b) Mn_3O_4 + 25% CNT and (c) Mn_3O_4 + 35% CNT.

Figure 2 shows a FESEM image of the samples. The powder of Mn_3O_4 itself has an average particle size of ~1 μm as shown in Figure 2(a). On the other hand, the small nano particles of Mn_3O_4 entered inside CNT particles and formed morphology like distal colon of rabbit due to sonication and hydrothermal treatment that degraded the particles of Mn3O4. So, CNT diameter without Mn_3O_4 has a diameter of 41.2 nm (Figure 2b) but samples with 25 and 35% CNT have 108.4 and 88.6 nm, respectively as shown in Figure 2c,d. Thus, 35% CNT has less particle size than 25% CNT. The preparation of Mn_3O_4 without using CNT gives agglomeration of the grains with large particle size. However, the use of CNT enhances the formation of nano-particles of Mn_3O_4 under ultrasonic technique. Similar reported results were published explaining that HRTEM (high resolution transmission electron microscope) images indicated the presence of the Mn_3O_4nano-particles enclosed and encapsulated within the carbon nanotubes [4].

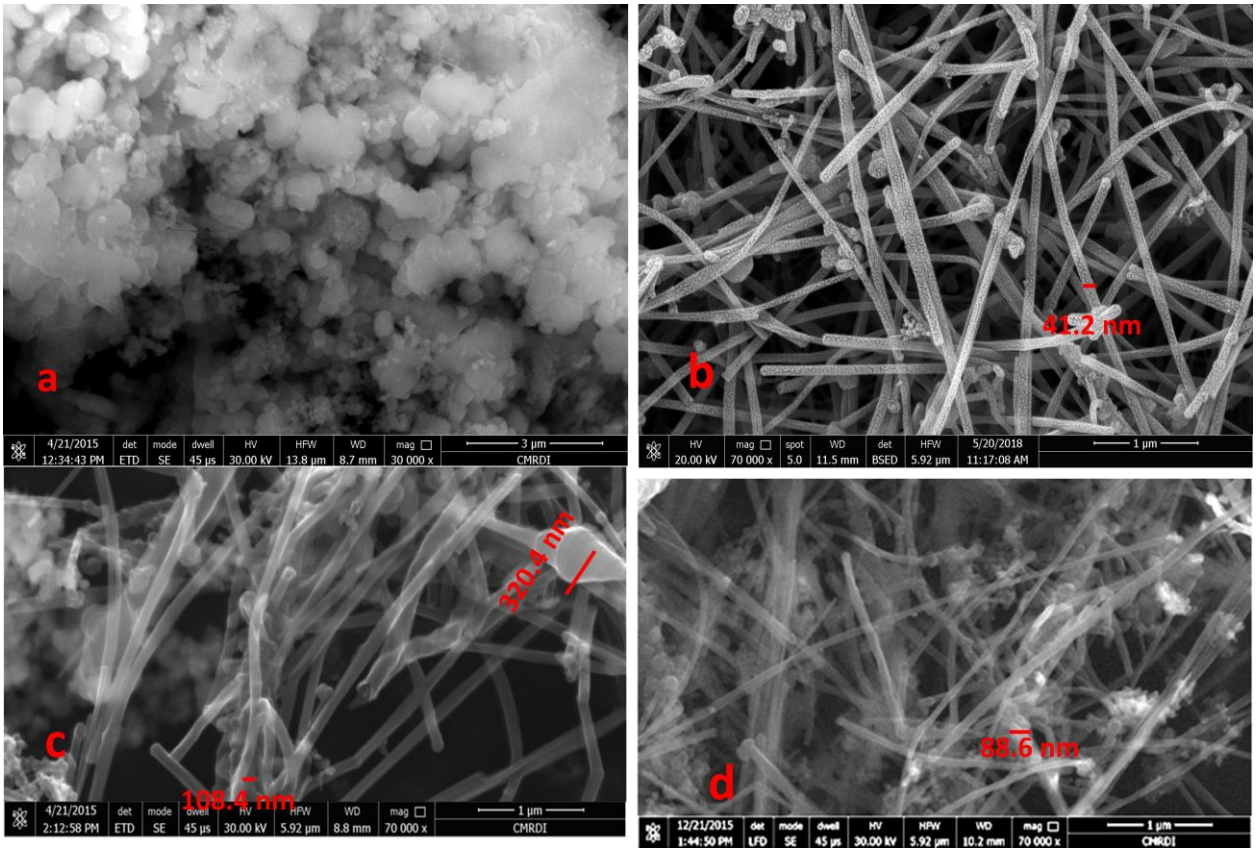

Figure 2. SEM of (a) Mn_3O_4, (b) CNT, (c) Mn_3O_4 + 25% CNT & (d) Mn_3O_4 + 35% CNT.

3.2. Electrochemical Impedance Spectroscopy and magnetic properties measurements

Electrochemical impedance spectroscopy (EIS) may be considered as one of the most sensitive tools for the study of differences in electrode behavior due to surface modification. The electrochemical impedance spectra of the cells, as presented in Figure 3, show an intercept at high frequency on the real axis Z' for the resistance of the electrolyte, R_e, followed by a semicircle in the high-middle frequency region, and a straight line in the low frequency region. The numerical value of the diameter of the semicircle on the Z_{real} axis is approximately equal to the charge transfer resistance, R_{ct}, and therefore, it can be seen that there is a marked decrease in Rct with the addition of CNT until 35% (R_{ct} =127 Ω), but 50% CNT increases R_{ct}, 928 Ω. So, the increase of CNT percentage decreases the R_{ct} until 35% CNT and after that the charge resistance increases again with the increase of CNT. i.e. 35% CNT is the optimum condition of these experiments.

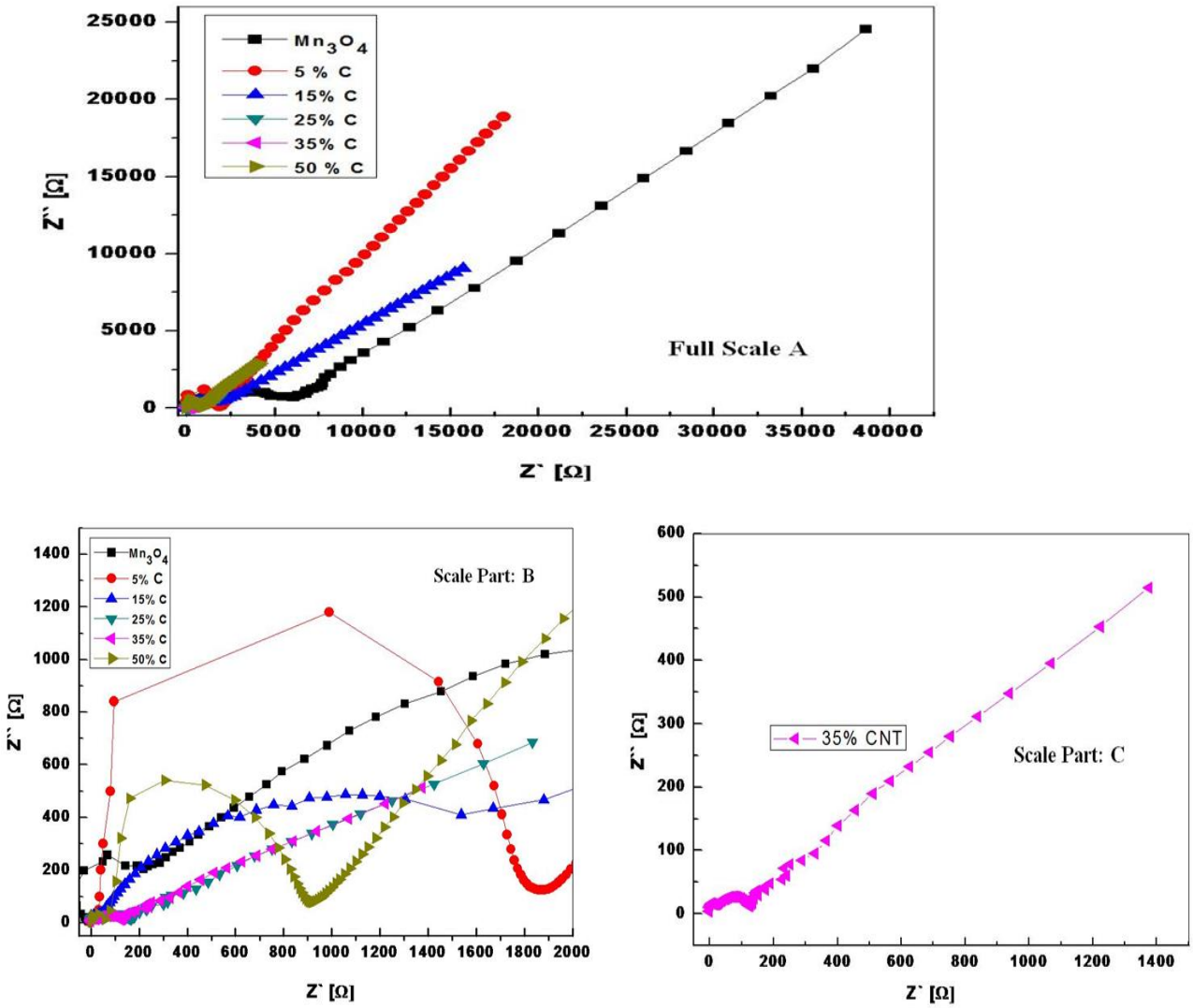

Figure 3. EIS of cells prepared from: (a) Mn_3O_4, (b) Mn_3O_4 + 5% CNT, (c) Mn_3O_4 + 15% CNT, (d) Mn_3O_4 + 25% CNT, (e) Mn_3O_4 + 35% CNT and (f) Mn_3O_4 + 50% CNT. Full Scale: A Scale Part B up to Z` = 2000 Ω and Scale Part C for Mn_3O_4 + 35% CNT only.

The straight line in the low frequency region is attributed to the diffusion of the lithium ions into the bulk of the electrode material, or the so-called Warburg diffusion. The plot of the real part of the impedance, Z re, versus the reciprocal root square of the lower angular frequencies is displayed in Figure 4.

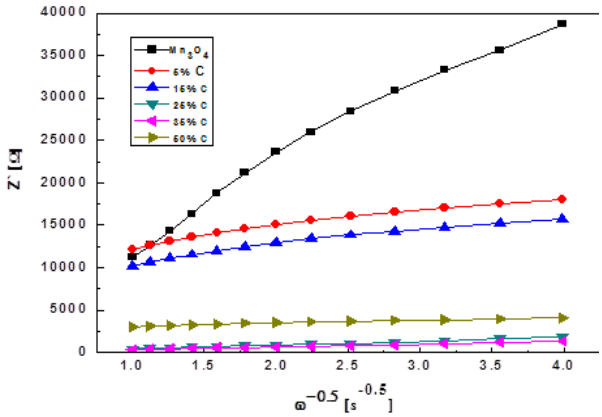

Figure 4. Relationship between real impedance with the low angular frequencies for Li/ Mn_3O_4-CNT cells.

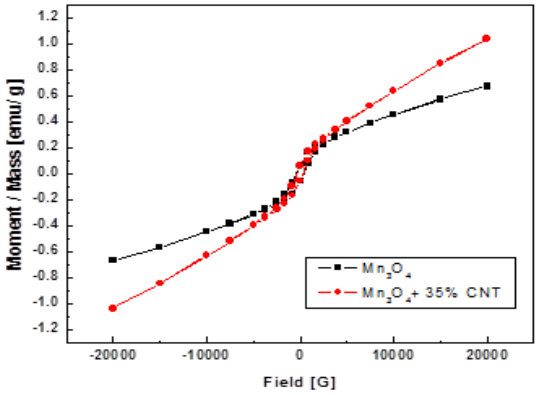

Figure 5. The relation between the magnetization and the magnetic field of the samples.

Table 1. Electrochemical Impedance parameters of of lithium cells using anodes prepared from Mn_3O_4 with and without different percentage of CNT.

Cell sample	R_{ct}[Ω]	σ_ω [Ω.$s^{0.5}$]	D[cm^2s^{-1}]	i° [A]	C_{dl} [F]
Mn_3O_4	6095.71	8182.5	5.29E-14	4.22E-06	1.64E-07
5% CNT	1872.9	1984.51	8.99E-13	1.37E-05	4.26E-10
15% CNT	1545.17	1841.95	1.04E-12	1.66E-05	8.18E-10
25% CNT	164.51	451.496	1.74E-11	1.56E-04	4.85E-07
35% CNT	127.0218	3.39E+02	3.09E-11	2.02E-04	6.28E-07
50% CNT	928	3.44E+02	2.99E-11	2.77E-05	1.36E-09

The straight lines are attributed to the diffusion of the lithium ions into the bulk of the electrode material, or the so-called Warburg diffusion. This relation is governed by equation 2. It is observed that the Warburg impedance coefficient, σ_w is 339 Ω.$s^{0.5}$ for cell composed from Mn_2O_3 with 35% CNT cell, and it is the lowest value among the other cells. The parameters of the electrochemical impedance spectroscopy are presented in Table 1. Also, the diffusion coefficient values of the lithium ions for diffusion into the bulk electrode materials have been calculated using Equation (3) and are recorded in Table 1.

$$Z_{re} = R_e + R_{ct} + \sigma_w .\omega^{-0.5} \quad (2)$$

$$D = 0.5\left(\frac{RT}{A\,F2\sigma w\,C}\right)^2 \quad (3)$$

$$Z_{re} = R_e + R_{ct} + 2\sigma_w{}^2.\, C_{dl} \quad (4)$$

The double layer capacitance is given by equation (5).

$$\omega = 1 / R_{ct}.C_{dl} \quad (5)$$

where: R_{ct}: charge transfer resistance, R_e: electrolyte resistance, ω: angular frequency in low frequency region, D: diffusion coefficient, R: the gas constant, T: the absolute temperature, F: Faraday's constant, A: the area of electrode surface, and C: molar concentration of Li^+ ions [2,15]. The obtained diffusion coefficient, 3.09x10^{-13} cm^2s^{-1} for Mn_3O_4 with 35% CNT cell explains the higher mobility for Li^+ ion diffusion than in the other cell. Furthermore, the exchange current density is given by the following formula:i° = RT/nFR_{ct}, where n is the number of electron involved in the electrochemical reaction. It is observed that C_{dl} for cell " $Mn_3O_4$with 35% CNT " has the highest value: 1.66 x 10^{-8} F.

The magnetic properties of Mn_3O_4 and Mn_3O_4 with 35% CNT samples are shown in Figure 5. It is observed that the magnetization of Mn3O4 with 35% CNT sample is higher than Mn_3O_4 one. The magnetic coercivities (Hc) are 322.98 and 365.39 G for samples without CNT and with 35% CNT, respectively as shown in Figure 5. This means that the presence of 35% C increases the H_c. i.e. Mn_3O_4 with 35% CNT is more ferromagnetic than Mn_3O_4 itself.

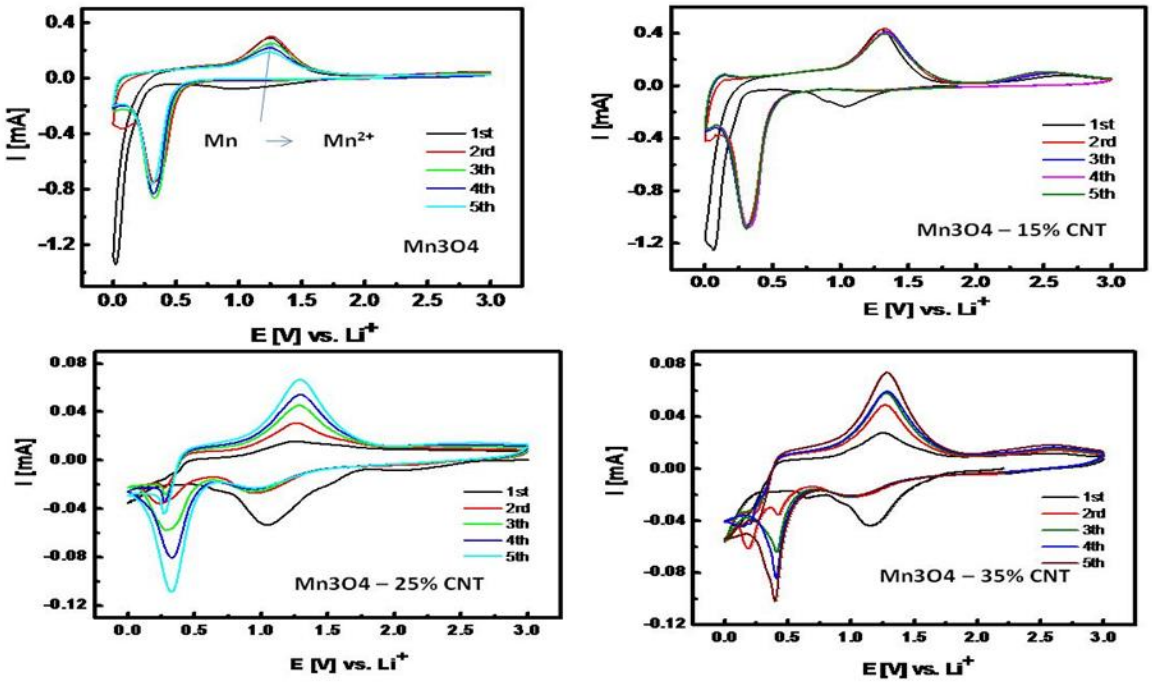

Figure 6. Cyclic voltammograms of Li/ Mn_3O_4-CNT cells.

3.3 Potentiodynamic and galvanostatic measurements

Cyclic voltammetric (CV) measurements were carried out between 0 and 3 V as shown in Figure 6. The cyclic voltammogram of the investigated Mn_3O_4 sample shows two cathodic reduction peaks at 0.9 (broad) and 0.3 V vs. Li+. The first peak for formation of a solid electrolyte interphase (SEI) film owing to the decomposition of electrolyte on the Mn_3O_4 particle surface and reduction of Mn^{3+} to Mn^{2+} [8], while the second one (0. 3V) for Mn^{2+} to Mn(0) and the formation of amorphous Li_2O based on the electrochemical conversion reaction as follows:

On the other hand, the anodic oxidation peaks take place at 1.3 and 2.6V vs. Li+. These peaks are attributed to the oxidation of Mn^0 to Mn^{2+} and the other is assigned to the re–oxidization of Mn^{2+} to higher oxidation state manganese [13]. It is observed that the addition of the CNT with 25 or 35% increases the current intensities of the peaks.

The first discharge/charge capacity plateaus versus the working voltage between 3 and 0.01V vs. Li^+ are shown in Figure 7. The first discharge capacities of the cells are nearly about 1050 $mAhg^{-1}$. The profiles for the first discharge curves look fairly similar for the investigated cells. There is a small transient and slope plateau between 1.5 and 0.25V vs. Li^+ for the formation of solid electrolyte interface (SEI) film and the reduction of Mn_3O_4 to Mn^{2+}, respectively. A plateau at 0.25 V is observed that corresponded to further reduction of Mn^{2+} to Mn(0) [7–9,16].

Figure 8 shows the curves of the specific discharge capacity vs. the cycle number of the different cells samples in the discharge voltage range of 3 and 0.01 V. For Li/ Mn_3O_4- 35% CNT cell, the capacity can be retained to about 90% of the discharge capacity after 100 cycles with respect to 2nd cycle and the specific discharge capacity is about 688 $mAhg^{-1}$, which is the highest value among the other cells. The initial capacity loss is attributed to the surface film formation, which is known as solid electrolyte interface (SEI) film. This is due the formation of irreversible reaction as: $8Li^+ + 8e^- + Mn_3O_4 \rightarrow 4Li_2O$

+ 3Mn [17,18]. It is observed from CV measurements (Figure 6) that the 2nd and the followed cycles of Mn_3O_4 have no cathodic reduction peaks at 1V butMn_3O_4 with 25 and 35% CNT have this type peak. This means that quasi-reversible of Mn_3O_4/CNT composite is formed as reported with similar Mn_3O_4/Graphite composite [17]. It can be explained that the reaction is an intercalation reaction when the discharge voltage was limited at 1.5V, the frame structure of material almost was not destroyed, and however, the reaction was a probable redox reaction when the discharge voltage went to lower potential (i.e. 1.5–0.01 V), then the structure of the materials is entirely destroyed at very low potential and cannot be recovered. It can be expected that the charge/discharge voltage is the key factor to affect the cyclic performance.

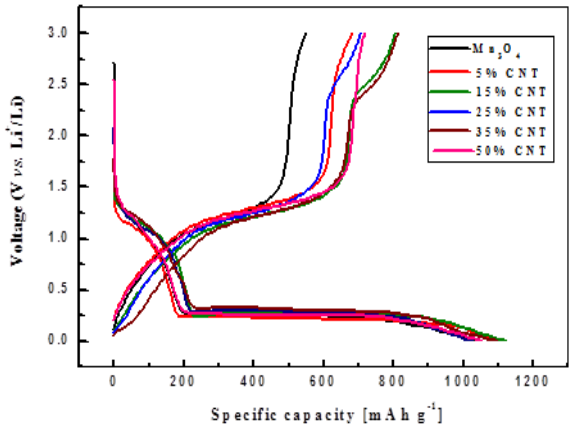

Figure 7. Capacity- voltage profile of Li/ Mn_3O_4-CNT cells.

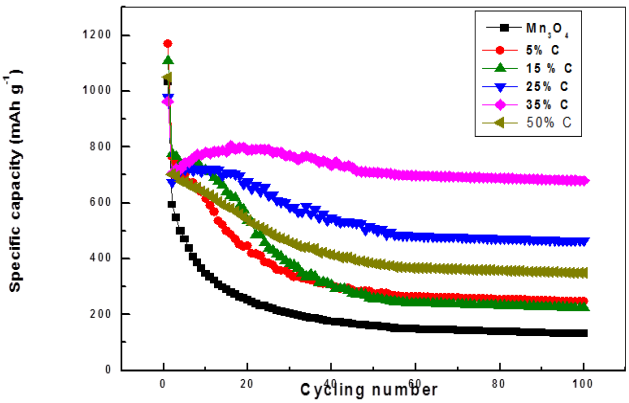

Figure 8. Cycle life performance of Li/ Mn_3O_4-CNT cells.

4. Conclusion

Different ratios of Mn_3O_4/CNT (carbon nano tubes) samples were prepared by hydrothermal reaction. Their crystal structures of the samples are tetragonal system. The cell of Mn_3O_4/35% CNT has lowest charge transfer resistance, R_{ct}, 19.18 Ω. The magnetic coercivities (H_c) are 322.98 and 365.39 G for samples without CNT and with 35% CNT, respectively. For Li/ Mn_3O_4- 35% CNT cell, the capacity can be retained to about 90% of the discharge capacity after 100 cycles and the specific discharge capacity is about 688 $mAhg^{-1}$, which is the highest among the other cells at discharge current density $0.02Acm^{-2}$.

References

[1] Wenelska K, Ottmann A, Schneider P, Thauer E, Klingeler R and Mijowska E 2016 Hollow carbon sphere/metal oxide nanocomposites anodes for lithium-ion batteries *Energy***103** 100–6
[2] Shenouda A Y and Liu H K 2010 Preparation, characterization, and electrochemical performance of Li2CuSnO4 and Li2CuSnSiO6 electrodes for lithium batteries *J. Electrochem. Soc.***157** A1183–7
[3] Shenouda A Y and Liu H K 2008 Electrochemical behaviour of tin borophosphate negative electrodes for energy storage systems *J. Power Sources***185** 1386–91

[4] Gangaraju D, Sridhar V, Lee I and Park H 2017 Graphene-carbon nanotube-Mn3O4 mesoporous nano-alloys as high capacity anodes for lithium-ion batteries *J. Alloys Compd.***699** 106–11
[5] Liang M and Zhi L 2009 Graphene-based electrode materials for rechargeable lithium batteries *J. Mater. Chem.***19** 5871–8
[6] Wang Z-H, Yuan L-X, Shao Q-G, Huang F and Huang Y-H 2012 Mn3O4 nanocrystals anchored on multi-walled carbon nanotubes as high-performance anode materials for lithium-ion batteries *Mater. Lett.***80** 110–3
[7] Yang Z, Lu D, Zhao R, Gao A and Chen H 2017 Synthesis of a novel structured Mn3O4@ C composite and its performance as anode for lithium ion battery *Mater. Lett.***198** 97–100
[8] Jing M, Hou H, Yang Y, Zhang Y, Yang X, Chen Q and Ji X 2015 Electrochemically alternating voltage induced Mn3O4/graphite powder composite with enhanced electrochemical performances for lithium-ion batteries *Electrochim. Acta***155** 157–63
[9] Luo S, Wu H, Wu Y, Jiang K, Wang J and Fan S 2014 Mn3O4 nanoparticles anchored on continuous carbon nanotube network as superior anodes for lithium ion batteries *J. Power Sources***249** 463–9
[10] Xu S-D, Zhu Y-B, Zhuang Q-C and Wu C 2013 Hydrothermal synthesis of manganese oxides/carbon nanotubes composites as anode materials for lithium ion batteries *Mater. Res. Bull.***48** 3479–84
[11] Park S-H and Lee W-J 2015 Hierarchically mesoporous carbon nanofiber/Mn3O4 coaxial nanocables as anodes in lithium ion batteries *J. Power Sources***281** 301–9
[12] Zhao Y, Ma C and Li Y 2017 One-step microwave preparation of a Mn3O4 nanoparticles/exfoliated graphite composite as superior anode materials for Li-ion batteries *Chem. Phys. Lett.***673** 19–23
[13] Cui X, Wang Y, Chen Z, Zhou H, Xu Q, Sun P, Zhou J, Xia L, Sun Y and Lu Y 2015 Preparation of pompon-like MnO/carbon nanotube composite microspheres as anodes for lithium ion batteries *Electrochim. Acta***180** 858–65
[14] Yang X, Wang X, Zhang G, Zheng J, Wang T, Liu X, Shu C, Jiang L and Wang C 2012 Enhanced electrocatalytic performance for methanol oxidation of Pt nanoparticles on Mn3O4-modified multi-walled carbon nanotubes *Int. J. Hydrogen Energy* **37** 11167–75
[15] Faulkner A J B and L R *Electrochemical Methods* (John Wiley & Sons, New York.)
[16] Fang X, Lu X, Guo X, Mao Y, Hu Y-S, Wang J, Wang Z, Wu F, Liu H and Chen L 2010 Electrode reactions of manganese oxides for secondary lithium batteries *Electrochem. commun.***12** 1520–3
[17] Hao Q, Wang J and Xu C 2014 Facile preparation of Mn 3 O 4 octahedra and their long-term cycle life as an anode material for Li-ion batteries *J. Mater. Chem. A* **2** 87–93
[18] Zhuang Y, Ma Z, Deng Y, Song X, Zuo X, Xiao X and Nan J 2017 Sandwich-like Mn3O4/carbon nanofragment composites with a higher capacity than commercial graphite and hierarchical voltage plateaus for lithium ion batteries *Electrochim. Acta* **245** 448–55.